Vibronic structure of VO_2 probed by slow photoelectron velocity-map imaging spectroscopy

Jongjin B. Kim, Marissa L. Weichman, and Daniel M. Neumark[a)]
Department of Chemistry, University of California, Berkeley, California 94720, USA and
Chemical Sciences Division, Lawrence Berkeley National Laboratory, Berkeley, California 94720, USA

(Received 29 November 2013; accepted 23 December 2013; published online 16 January 2014)

We report high-resolution anion photoelectron spectra of vanadium dioxide (VO_2^-) obtained by slow electron velocity-map imaging of trapped and cryogenically cooled anions. Vibrationally resolved spectra are obtained for photodetachment to the first three neutral electronic states, giving an electron affinity of 1.8357(5) eV for the $\tilde{X}\,^2A_1$ ground state and term energies of 0.1845(8) eV and 0.8130(5) eV for the $\tilde{A}\,^2B_1$ and $\tilde{B}\,^2A_1$ excited states, respectively. The vibrational fundamentals ν_1 and ν_2 are obtained for all three states. Experimental assignments are confirmed by energies from electronic structure calculations and Franck-Condon spectral simulations. These simulations support assigning the anion ground state as the $\tilde{X}\,^3B_1$ state. With this assignment, photodetachment to the $\tilde{B}\,^2A_1$ state involves a nominally forbidden two-electron transition, suggesting extensive configuration interaction in neutral VO_2. © *2014 AIP Publishing LLC*. [http://dx.doi.org/10.1063/1.4861667]

I. INTRODUCTION

Vanadium oxides are among the most versatile metal oxide catalysts used in industry.[1,2] Supported vanadia catalysts play a key role in the oxidative dehydrogenation of propane and the oxidation of methanol, two processes of considerable industrial importance.[3,4] In addition, bulk vanadium dioxide undergoes an insulator-to-metal transition just above room temperature that can also be driven by optical excitation; this property has attracted great interest for sensor development and electronic switching technology.[5–7] These applications have motivated experimental and theoretical efforts aimed at understanding how the molecular-level properties of vanadium oxide catalysts govern their catalytic activity.[8–10] In particular, as the reactivity of supported catalysts is known to depend on the size of small catalyst particles,[11,12] there has been a focus on the chemistry of gas-phase size-selected vanadium oxide clusters as model catalytic systems.[13–16] We add to this foundation by using high-resolution anion photoelectron spectroscopy to unravel the complex vibronic structure of triatomic VO_2.

Numerous investigations of vanadium oxide clusters have focused on their reactivity and structure. The products of ionic vanadium oxide clusters with various possible reactants have been characterized using tandem mass spectrometry techniques.[13,17–19] Reactivity studies of gas-phase neutral clusters have been performed with a flow reactor coupled to a photoionization mass spectrometer.[20–22] IR absorption spectroscopy has also been used to determine the products of VO_2 with acetylene and hydrogen isolated in an inert gas matrix.[23,24] These experiments have demonstrated a rich size- and charge-dependent chemistry for isolated vanadium oxide clusters.

The reactivity studies have relied primarily on theoretical calculations for interpreting the mechanisms in terms of the electronic and geometric changes through the course of a reaction. Transition metal compounds, however, have proven difficult to model correctly, owing to multiple low-lying isomers, relatively few reliable experimental benchmarks, multireference character, and a large orbital active space.[25,26] A very fruitful approach combining experiment and theory to investigate the structure and reactivity of anionic and cationic vanadium oxide clusters has been carried out by Asmis, Sauer, and co-workers using various IR photodissociation (IRPD) methods combined with ion cooling.[14,27] By comparing the IR spectra with electronic structure calculations, they successfully identified the structures of numerous anionic and cationic vanadium oxide clusters. They also found that the larger clusters often had polyhedral structures, a completely different motif than that observed in bulk vanadium oxides. Characteristic IR absorption bands were also associated with particular structural moieties, aiding in the interpretation of IR spectra of other vanadium oxide clusters.

Transition metal compounds often have complex electronic structure and numerous low-lying excited electronic states that can play an important role in reaction mechanisms;[28] vanadium oxide species are no exception. The smallest vanadium oxide, the diatomic VO, has a well-studied but complicated rovibronic structure, with at least 14 experimentally identified electronic states.[29,30] The next larger molecular species is triatomic VO_2. Ground-state properties of neutral VO_2 have been calculated by complete active space self-consistent field (CASSCF) theory,[31] several different implementations of density functional theory (DFT),[32–37] quantum Monte Carlo, and coupled-cluster theory.[38] The properties of the anions have also been investigated by many of the same methods.[32,34,37] Most calculations agree that VO_2 and its anion have a bent C_{2v} structure, but different methods obtain different electronic ground states. Calculations find

a)Author to whom correspondence should be addressed. Electronic mail: dneumark@berkeley.edu

neutral VO_2 to have a $^2A_1$ or $^2B_1$ ground state,[31–34,38] while the anion VO_2^- has been calculated to have either a $^3A_1$ or $^3B_1$ ground state.[32,34,37]

A few spectroscopic studies have been performed on neutral and anionic VO_2. The first was an electron paramagnetic spectroscopy study of VO_2 isolated in a rare gas matrix.[31] Analysis of the spectra confirmed a $^2A_1$ ground state for neutral VO_2. IR spectroscopy of matrix-isolated VO_2 has identified ν_1 and ν_3 vibrational fundamentals.[34,39] Anion photoelectron (PE) spectra have been measured for VO_2^-.[40] The electron affinity (EA) and excited state term energies of VO_2 were determined, though there was minimal observation of vibrational structure owing to the energy resolution of the experiment (~30 meV) and possible contributions from hot bands. Partially resolved features near the assigned origin transition, however, suggested the presence of photodetachment from thermally populated low-lying excited anion states. Although Asmis and co-workers have measured IRPD spectra of various mass-selected vanadium oxide ionic clusters including the cation VO_2^+,[41] they have not reported any IR spectra of VO_2^-.

In this work, we investigate the anion PE spectroscopy of VO_2 with enhanced ion cooling and resolution, using slow electron velocity-map imaging (SEVI)[42] combined with a cryogenic ion trap.[43] This method yields sub-meV energy resolution with minimal complications from the hot bands that have complicated previous studies of metal oxide clusters by photoelectron spectroscopy.[44,45] We observe fully vibrationally resolved transitions from the anion ground state to the first three electronic states of neutral VO_2. Assignments are confirmed with the aid of Franck-Condon simulations and electronic structure calculations. The improved resolution and ion cooling allows us to obtain accurate vibrational frequencies, electron affinities, and term energies. We also reassign bands observed in the previously reported anion PE spectra[40] to be consistent with our interpretation.

II. EXPERIMENTAL

The high-resolution SEVI anion photoelectron spectroscopy apparatus has been described in detail previously.[42,43,46] A cryogenic ion trap ensures that the ions of interest are cooled to their ground vibrational state, regardless of the method of ion production. SEVI uses a velocity-map imaging (VMI) electron spectrometer[47] at low extraction voltages to acquire photoelectron spectra at low kinetic energies and thus at high resolution.

Vanadium oxide cluster anions were produced by laser ablation of a solid vanadium target. A 2–10 mJ pulse of 532 nm light was focused onto the surface of a vanadium disc. Helium gas from a pulsed valve quenched the plasma and entrained the resulting charged and neutral clusters. Trace oxygen in the gas lines and residual oxide on the surface were sufficient for the production of VO_2^- anions. The gas expansion and ion optics directed the anions through a RF hexapole ion guide and quadrupole mass filter into a cryogenic octupole ion trap held at 5 K. There, the ions were cooled by a 20:80 H_2:He buffer gas mix for 40 ms to their ground vibrational state and as cold as 10 K.[43]

After cooling in the ion trap, the ions were extracted into a time-of-flight mass spectrometer. Upon reaching the VMI interaction region, the VO_2^- ion packets were photodetached by the output of a Nd:YAG-pumped tunable dye laser. Photoelectrons were collected and projected onto the detection plane by the VMI electrostatic lens, and the resulting electron events were recorded by an imaging detector comprising two microchannel plates coupled to a phosphor screen.[48] The radial and angular distributions were reconstructed from the projected image by an inverse-Abel algorithm,[49] with the axis of cylindrical symmetry set by the laser polarization.

The radial distribution gives the electron velocity distribution and hence the electron kinetic energy (eKE) spectrum. The electron spectrometer was calibrated with the well-characterized detachment transitions of O^- and S^-.[50,51] The energy resolution is given by ΔeKE. The resolving power eKE/ΔeKE is approximately constant, so the best resolution is obtained at smallest eKE. SEVI uses relatively low extraction voltages on the VMI electrode stack, resulting in an expanded view of the high-resolution, low-eKE portion of a given photoelectron image. As the highest resolution is achieved at the low-eKE portion of a given image, a complete set of high-resolution spectra was acquired by tuning the laser frequency in steps such that each transition of interest had a corresponding high-resolution spectrum. Individual scans were combined by taking the high-resolution portion of each and scaling them to the appropriate low-resolution overview spectrum, as threshold effects may distort peak intensities at low eKE.[52] Spectra are typically plotted as a function of the electron binding energy (eBE) given by $\text{eBE} = h\nu - \text{eKE}$, as this quantity is intrinsic to the species of interest and independent of the photon energy.

SEVI spectra of the atomic calibration systems can yield peak widths as narrow as 1 cm^{-1},[46] but no peaks narrower than 10 cm^{-1} were seen in the VO_2^- SEVI spectra. As was the case in the spectra of the Group 4 dioxides,[53] the peak widths are wider than in previous cryo-cooled SEVI spectra[54,55] due to larger rotational constants and thus wider unresolved rotational structure.

The images also yield the photoelectron angular distribution (PAD). For one-photon detachment, the PAD is given by the form,

$$\frac{d\sigma}{d\Omega} = \frac{\sigma_{tot}}{4\pi}\left(1 + \beta\left(\frac{3}{2}\cos^2\theta - \frac{1}{2}\right)\right), \quad (1)$$

where θ is the angle of the ejected electron relative to the polarization of the photodetachment laser. The anisotropy parameter β varies from −1 to 2, corresponding to the limits where the electron distribution is aligned perpendicular and parallel to the laser polarization.[56,57] As its value is not constant but depends on eKE, which can vary by over an order of magnitude across different high-resolution scans, numerical values are not listed.[56,58] However, for a given detachment transition, β is often predominantly only positive or negative-to-zero over a wide range of eKE. Peaks with $\beta > 0.2$ are labeled with a "+" PAD while those with $\beta < 0.2$ have a "−" PAD.

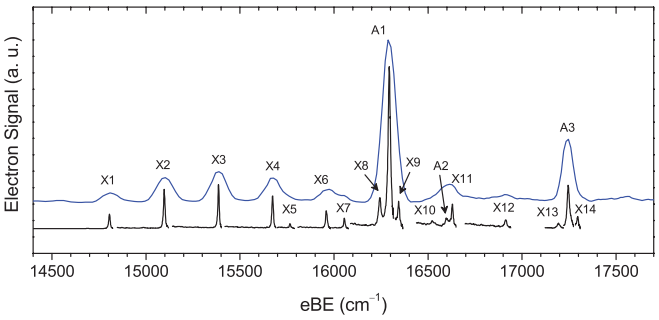

FIG. 1. SEVI spectra of the photodetachment of VO_2^- to the $\tilde{X}\,^2A_1$ and $\tilde{A}\,^2B_1$ neutral states. The upper blue trace is a low-resolution overview spectrum and the lower black traces are segments of high-resolution scans covering the range of the overview scan.

III. RESULTS

Photoelectron spectra of VO_2^- are presented in Figs. 1 and 2, covering two different ranges of eBE. Lower-resolution overview spectra are displayed on top (blue), taken at photon energies of 19 226 cm^{-1} in Fig. 1 and 23 520 cm^{-1} in Fig. 2. High-resolution SEVI spectra are spliced together underneath (black), with photon energies chosen to maximize energy resolution for the transitions of interest in each scan.

The overview spectrum in Fig. 1 covers about 3000 cm^{-1}. It shows a series of approximately equally spaced peaks X1–X6 and two considerably more intense peaks, A1 and A3. The overall appearance of this band suggests that it includes two electronically distinct photodetachment transitions. The higher resolution spectra in Fig. 1 show the underlying vibrational structure in more detail, and reveal that several of the transitions in the overview spectrum consist of two or more closely spaced peaks. Three vibrational progressions are evident. Two progressions have a characteristic peak spacing of ∼290 cm^{-1}. Peaks X1–X4, X6, X8, and X10 comprise one progression, and a second progression with similar spacing is composed of peaks X5, X7, X9, X11, X12, and X13. The two progressions are offset by ∼960 cm^{-1}. Peak X14 lies another 952 cm^{-1} above peak X9. This structure is characteristic of vibrational activity in only two modes in the neutral VO_2 upon photodetachment. Finally, peaks A1 and A3 are separated by 952 cm^{-1} and do not appear to be associated with the other two progressions.

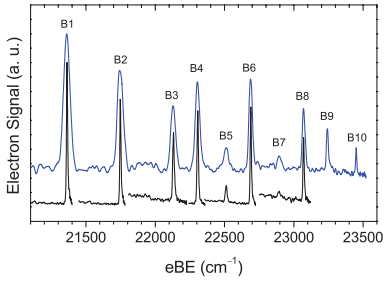

FIG. 2. SEVI spectra of the photodetachment of VO_2^- to the $\tilde{B}\,^2A_1$ neutral state. The upper blue trace is a low-resolution overview spectrum and the lower black traces are segments of high-resolution scans covering the range of the overview scan.

TABLE I. Peak positions (cm^{-1}), shifts from respective origins (cm^{-1}), and vibronic assignments for the VO_2^- SEVI spectra.

Peak	eBE	Offset	Assignment	Neutral state
X1	14 806	0	0_0^0	$\tilde{X}\,^2A_1$
X2	15 097	291	2_0^1	$\tilde{X}\,^2A_1$
X3	15 386	580	2_0^2	$\tilde{X}\,^2A_1$
X4	15 673	868	2_0^3	$\tilde{X}\,^2A_1$
X5	15 766	960	1_0^1	$\tilde{X}\,^2A_1$
X6	15 960	1154	2_0^4	$\tilde{X}\,^2A_1$
X7	16 055	1249	$1_0^1 2_0^1$	$\tilde{X}\,^2A_1$
X8	16 244	1438	2_0^5	$\tilde{X}\,^2A_1$
A1	16 294	0	0_0^0	$\tilde{A}\,^2B_1$
X9	16 343	1537	$1_0^1 2_0^2$	$\tilde{X}\,^2A_1$
X10	16 524	1718	2_0^6	$\tilde{X}\,^2A_1$
A2	16 600	306	2_0^1	$\tilde{A}\,^2B_1$
X11	16 629	1823	$1_0^1 2_0^3$	$\tilde{X}\,^2A_1$
X12	16 913	2107	$1_0^1 2_0^4$	$\tilde{X}\,^2A_1$
X13	17 194	2388	$1_0^1 2_0^5$	$\tilde{X}\,^2A_1$
A3	17 246	952	1_0^1	$\tilde{A}\,^2B_1$
X14	17 295	2489	$1_0^2 2_0^2$	$\tilde{X}\,^2A_1$
B1	21 363	0	0_0^0	$\tilde{B}\,^2A_1$
B2	21 748	385	2_0^1	$\tilde{B}\,^2A_1$
B3	22 132	768	2_0^1	$\tilde{B}\,^2A_1$
B4	22 307	943	1_0^1	$\tilde{B}\,^2A_1$
B5	22 512	1149	2_0^3	$\tilde{B}\,^2A_1$
B6	22 690	1326	$1_0^1 2_0^1$	$\tilde{B}\,^2A_1$
B7	22 893	1529	2_0^4	$\tilde{B}\,^2A_1$
B8	23 071	1707	$1_0^1 2_0^2$	$\tilde{B}\,^2A_1$
B9	23 243	1879	1_0^2	$\tilde{B}\,^2A_1$
B10	23 450	2087	$1_0^1 2_0^3$	$\tilde{B}\,^2A_1$

The vibrational structure of the band within Fig. 2 is also indicative of vibrational activity in two modes upon photodetachment. Peaks B1–B3, B5, and B7 are spaced by ∼380 cm^{-1}, as are peaks B4, B6, B8, and B10. The two progressions, in turn, are offset by ∼940 cm^{-1}. The last peak B9 is offset from the origin B1 by 1879 cm^{-1}, twice the spacing between the two progressions. All observed transitions in all three bands have a PAD with positive β.

Peak positions and assignments are summarized in Table I. The peaks are wider than the instrumental resolution owing to unresolved rotational structure. Due to the uncertainty in the nature of this unresolved structure, errors in peak positions are given by $\pm\sigma$ of a Gaussian fit to a given vibronic transition, typically 4–6 cm^{-1} in this experiment.

IV. CALCULATIONS

Although metal oxide systems are often formally considered ionic, covalent molecular orbital theory has proven a useful framework for understanding the electronic structure of the 3*d* transition metal monoxides,[29] and is used here as a starting point for elucidating the relevant electronic states of neutral and anionic VO_2. The ground state configuration of atomic V is $4s^2 3d^3$. In VO_2 and VO_2^-, the formal oxidation state of the vanadium atom is +4 and +3, leaving one and two metal-centered valence electrons in the neutral and anion, respectively. The frontier orbitals to consider are the vanadium 3*d* and 4*s* orbitals interacting with the oxygen 2*p*

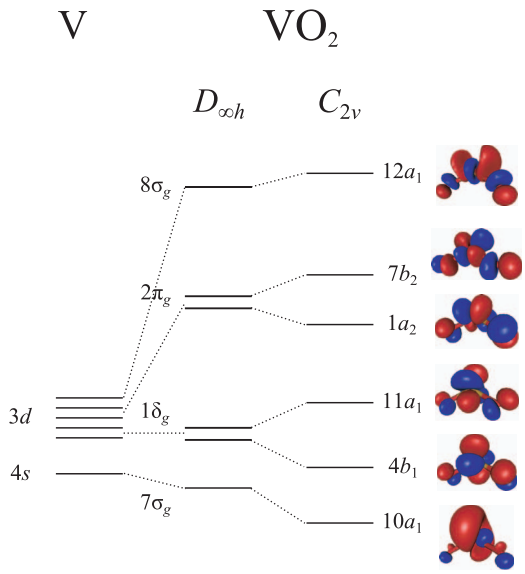

FIG. 3. Schematic orbital level diagram from the atomic vanadium (left) to the linear $D_{\infty h}$ VO_2 (center) to bent C_{2v} (right). As the diagram is only schematic, orbital energies are not to scale. Molecular orbitals are from the natural orbitals from the CASSCF calculation described in Sec. IV.

TABLE II. Calculated geometries, vibrational frequencies, and relative energies of the lowest-lying anion and neutral VO_2 states at BPW91/LANL2TZ and B3LYP/LANL2TZ.

	Anion			Neutral		
	$\tilde{X}\,^3B_1$	$\tilde{A}\,^3A_1$	$\tilde{a}\,^1A_1$	$\tilde{X}\,^2A_1$	$\tilde{A}\,^2B_1$	$\tilde{B}\,^2A_1$
			BPW91			
R (Å)	1.664	1.666	1.636	1.622	1.629	1.614
θ (deg)	119.6	121.8	108.4	110.8	119.4	113.2
ν_1 (cm^{-1})	895	894	959	984	969	981
ν_2 (cm^{-1})	278	281	354	315	304	382
ν_3 (cm^{-1})	910	909	946	973	980	1001
EA (eV)				1.79		
T_0 (eV)		0.07	0.51		0.23	0.95
			B3LYP			
R (Å)	1.660	1.662	1.628	1.617	1.619	
θ (deg)	123.4	125.1	109.8	115.8	121.5	
ν_1 (cm^{-1})	913	916	983	1018	1011	
ν_2 (cm^{-1})	274	278	349	268	305	
ν_3 (cm^{-1})	935	936	975	999	1015	
EA (eV)				2.09		
T_0 (eV)		0.04	0.71		0.10	

orbitals. In the covalent limit, the vanadium orbital energies are taken from the ionization potentials of the neutral vanadium atom instead of the ionic metal as in crystal field theory, resulting in $3d$ orbitals starting slightly higher in energy than the $4s$ orbital.[59] In linear VO_2, the $3d$ orbitals are split into a nonbonding δ_g orbital and higher-lying π_g and σ_g orbitals, as illustrated in Fig. 3. The lowering of symmetry to C_{2v} lifts the $3d$ orbital degeneracy further. The $1\delta_g$ orbital is split into the $4b_1$ and $11a_1$ orbitals, and the $2\pi_g$ orbital becomes the $1a_2$ and $7b_2$ orbitals. The $3d$ $11a_1$ orbital now has the same symmetry as the energetically close $4s$ $10a_1$ orbital, and the a_1 levels repel each other as illustrated in Fig. 3. Here we use the Mulliken convention,[60] in which a b_1 orbital is antisymmetric with respect to reflection in the plane of the molecule while a b_2 orbital is symmetric.

With this background, we can now make predictions for the anion and neutral electronic states of VO_2. The three lowest-lying neutral states correspond to the lone unpaired electron in the d^1 neutral occupying the $10a_1$, $4b_1$, or $11a_1$ orbitals, resulting in term symbols of $^2A_1$, $^2B_1$, and $^2A_1$, respectively. Similarly, the anion has an electron count of d^2, and three likely electron configurations for the ground state, $\ldots(10a_1)^2$, $\ldots(10a_1)(4b_1)$, and $\ldots(10a_1)(11a_1)$, corresponding to $^1A_1$, $^3B_1$, and $^3A_1$ term symbols, respectively.

Previous theoretical studies of vanadium oxide clusters have used the BPW91[61,62] and B3LYP[63] density functionals to obtain geometries, electronic states, and vibrational frequencies. B3LYP was successfully used in comparison with experimental IRPD results of various vanadium oxide clusters.[14,27,64] Although not compared directly with experiments on larger clusters, BPW91 has given similar predictions as B3LYP for the structures of clusters.[33,64,65] Many different density functional methods have been compared for applicability in transition metal and metal oxide systems.[25] No clear consensus has been made on the relative merits of different functionals, although it is believed that pure density functionals like BPW91 are more reliable for multireference systems than B3LYP, which includes some Hartree-Fock exchange.

To improve confidence in the theoretical results, both the B3LYP and BPW91 functionals are used to calculate the anion and neutral VO_2 energies, geometries, and vibrational frequencies. The triple-zeta LANL2TZ basis set combined with the Hay and Wadt effective core potentials are used for the vanadium atom, while the 6-311+G* basis set is used for the oxygen atoms.[66,67] The first two excited states are calculated with the maximum overlap method (MOM),[68] or with the ground state method if the excited states have different spin multiplicities. All density functional calculations were performed with Q-Chem 4.0,[69] and results are summarized in Table II.

As predicted by the simple molecular orbital model, the lowest states of the anion are the $^1A_1$, $^3B_1$, and $^3A_1$ states. Both density functionals predict an adiabatic energy difference between the two triplets less than 75 meV (2 kcal/mol). Although both methods give the $^3B_1$ state as the ground state, given the accuracy of DFT for challenging transition metal species, either triplet could be the ground state,[25] especially since two previous calculations using B3LYP and only varying the basis set found either the $^3A_1$ or $^3B_1$ state to be the ground state.[34,37] The singlet, however, is calculated to lie at least 0.5 eV above the ground state.[32] It is unlikely to be populated in this experiment and will not be considered further.

The lowest calculated states of the neutral VO_2 are $^2A_1$ and $^2B_1$ states, consistent with the MO ordering in Fig. 3. Calculations with either functional find that the $^2B_1$ state lies above the $^2A_1$ state, by 0.23 eV using BPW91 and 0.10 eV using B3LYP. The next excited state with the BPW91 functional is another $^2A_1$ state. However, that same state calculated by B3LYP undergoes root flipping and converges to the ground state. The consistency of ordering for all other states, however, suggests that the second excited state is a $^2A_1$ state.

Multireference *ab initio* calculations can provide insight into interactions between close-lying electronic states of the same symmetry found by DFT, an issue of interest discussed in Sec. V C. Although a proper accounting of dynamical electron correlation with multireference methods is beyond the scope of this paper, complete active-space self-consistent field theory (CASSCF) can be used to account for static correlation effects. Due to the lack of dynamical correlation, CASSCF calculations are only used to aid in interpretation of states obtained by DFT. For the neutral VO_2, the active space was 13 electrons in 12 orbitals, comprising the 3*d* and 4*s* vanadium orbitals along with the 2*p* oxygen orbitals. The basis sets and effective core potential were the same as used in the DFT calculations. CASSCF calculations were performed with Molpro 2010.1.[70]

To aid in the assignment of the photodetachment transitions, particularly the identification of the anion ground state, Franck-Condon (FC) simulations are calculated from the two triplet anion states to the three neutral states. BPW91 and B3LYP give qualitatively similar geometry changes upon electron detachment, thus the calculated FC spectra should be similar with the results from either method. Since B3LYP fails to give a stable solution for the excited $^2A_1$ state, the BPW91/LANL2TZ geometries, normal modes, and vibrational frequencies are used for an internally consistent set of FC simulations. FC simulations are generated using the ezSpectrum program,[71] which calculates FC intensities in the harmonic oscillator approximation but with full Duschinsky mixing of the normal modes.[72]

V. DISCUSSION

A. Assignments

Assignments are made based on peak positions and intensities; the PADs for all peaks are insufficiently distinguishable to differentiate between electronic states. The vibrational progressions in Figs. 1 and 2 are characteristic of three electronically distinct photodetachment transitions, each with two active vibrational modes. Though photodetachment transitions of multiple isomers have been observed in PE spectra of other metal dioxide anions,[73] previous calculations suggest that the other likely isomers, which have a peroxo or superoxo moiety, would have an EA of 1 eV or less.[32] No photodetachment signal was observed at those low binding energies, and thus all bands are attributed to the VO_2^- dioxo isomer. Ion trapping and cooling should ensure that the anion is in the ground electronic and vibrational state, so it is reasonable to assign the three bands to photodetachment from the anion ground state to the first three electronic states of neutral VO_2, an assumption tested in the following discussion. For a C_{2v} bent triatomic, the ν_1 VO symmetric stretch and the ν_2 OVO bend are totally symmetric and expected to be the two active modes within the FC approximation.

Peak X1 is assigned the vibrational origin of the $\tilde{X}\,^2A_1$ ground state, as no structure is visible at lower binding energies. Furthermore, the EA is calculated to be 1.79 eV by the BPW91 functional, in good agreement with the eBE of peak X1 at 1.8357(5) eV. The first progression of ~290 cm^{-1} consists of peaks X1-X4, X6, X8, and X10. The calculated frequency of the bending mode in the neutral ground state lies within 30 cm^{-1} of this spacing (Table II), so this set of peaks is assigned to the 2_0^n (n = 0–6) progression. Offset by 960 cm^{-1} from this progression is the series of peaks X5, X7, X9, X11, X12, and X13, with almost identical spacing within this series. The calculated symmetric stretch frequency is 984 cm^{-1} for the $\tilde{X}\,^2A_1$ state, so this second series of peaks is assigned to the $1_0^1 2_0^n$ (n = 0–5) progression. Peak X14 lies 952 cm^{-1} above the $1_0^1 2_0^2$ transition and, accounting for anharmonicity and its weak intensity, is assigned to the $1_0^2 2_0^2$ transition.

Neither the positions nor intensities of peaks A1, A2, and A3 can be fit assuming they are transitions to the $\tilde{X}\,^2A_1$ ground state. They are assigned as photodetachment to the $\tilde{A}\,^2B_1$ state of VO_2, with A1 as the vibrational origin. The experimental term energy is 0.1845(8) eV, a good match with the calculated value of 0.23 eV by BPW91. Peaks A2 and A3 are offset by 306 cm^{-1} and 952 cm^{-1} from A1, respectively. These values are in close agreement with the calculated frequencies for the ν_2 and ν_1 modes of the $\tilde{A}\,^2B_1$ state, so these peaks are assigned as the 2_0^1 and 1_0^1 transitions, respectively. The experimental resolution is high enough to show clearly that the two vibrational frequencies extracted from peaks A1–A3 are close to but different from the experimental frequencies of the $\tilde{X}\,^2A_1$ state. Hence, these peaks are clearly from transitions to a different neutral state, rather than transitions to the same neutral state from a different anion state. This observation is significant given the presence of two nearly degenerate $^3B_1$ and $^3A_1$ triplet states of the anions.

As mentioned earlier, the observed vibrational structure in the highest-eBE band comprises two progressions of ~380 cm^{-1} offset by ~940 cm^{-1}. Just as in the $\tilde{X}\,^2A_1$ bands, these are assigned to the 2_0^n (n = 0–4) and $1_0^1 2_0^n$ (n = 0–3) vibrational progressions. The origin of this band, B1, has an eBE of 21 363 cm^{-1}, giving a term energy of 0.8130(5) eV. This value is reasonably close to that calculated for the $\tilde{B}\,^2A_1$ state, 0.95 eV. Moreover, while the calculated and experimental ν_1 frequencies for the $\tilde{X}$, $\tilde{A}$, and $\tilde{B}$ states are very similar, the calculated ν_2 frequency of the $\tilde{B}\,^2A_1$ state is 70–80 cm^{-1} higher than those of the other two neutral states, in agreement with the observed bend frequency. This band is thus assigned as photodetachment to the $\tilde{B}\,^2A_1$ state. The remaining peak B9 is further offset from B4, the 1_0^1 transition, by 936 cm^{-1}, and is assigned by extrapolation to the 1_0^2 transition.

The assigned EAs, adiabatic term energies, and vibrational frequencies are summarized in Table III. As the extended 2_0^n progressions exhibit noticeable anharmonicity, the vibrational frequencies reported are the

TABLE III. Experimental vibrational fundamentals and electronic state energies for VO_2.

	$\tilde{X}\,^2A_1$	$\tilde{A}\,^2B_1$	$\tilde{B}\,^2A_1$
ν_1 (cm^{-1})	960(3)	952(6)	943(5)
ν_2 (cm^{-1})	291(2)	306(6)	385(4)
EA (eV)	1.8357(5)		
T_0 (eV)		0.1845(8)	0.8130(5)

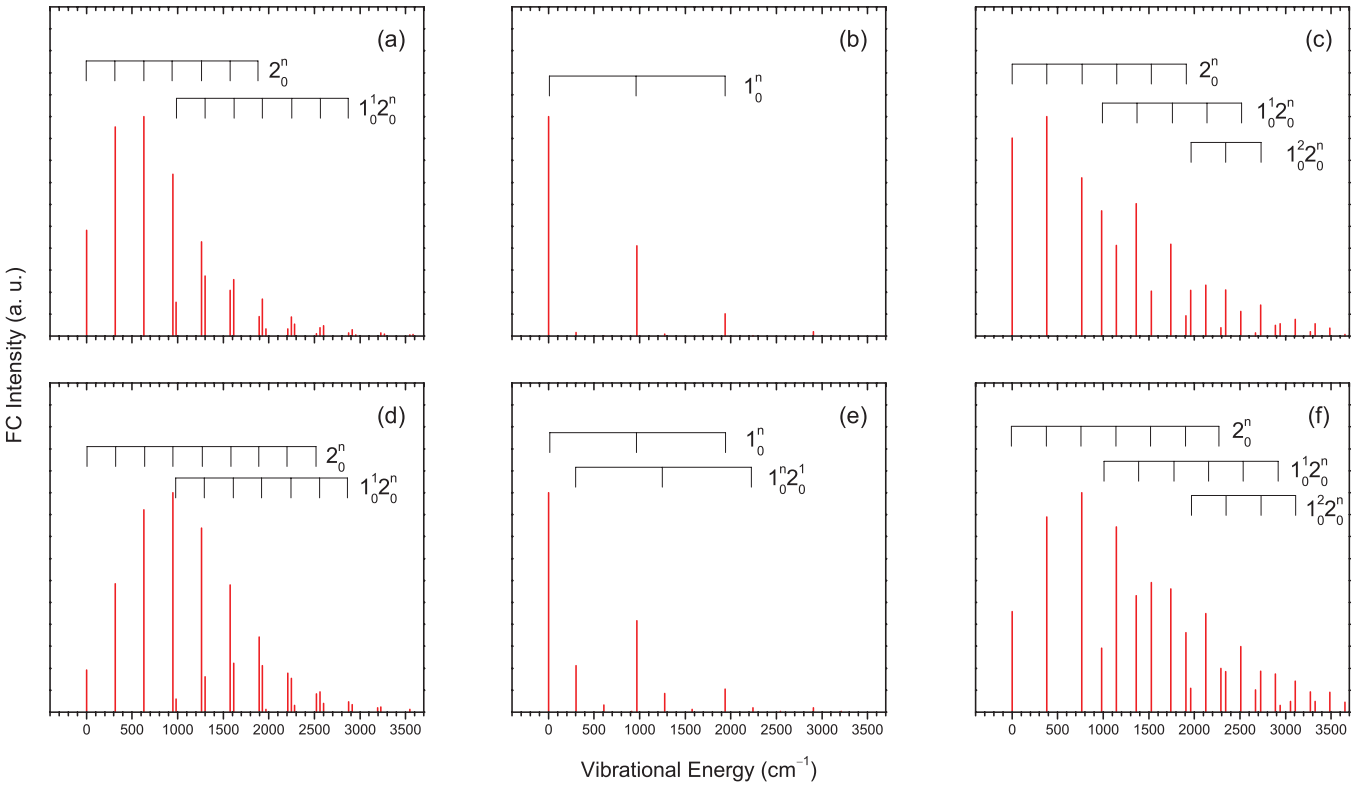

FIG. 4. Calculated FC intensities for the transitions from the lowest two anion electronic states to the three lowest neutral electronic states of VO_2. Panels (a), (b), and (c) are the calculated spectra for the transitions from the $^3B_1$ anion to the $\tilde{X}\,^2A_1$, $\tilde{A}\,^2B_1$, and $\tilde{B}\,^2A_1$ states, respectively. Panels (d), (e), and (f) are the calculated spectra to the same three neutral states from the $^3A_1$ anion state.

fundamentals. By fitting the $\tilde{X}\,^2A_1$ and $\tilde{B}\,^2A_1$ 2_0^n progressions to a Morse potential, we also obtain $\omega_2 = 292(2)\,\text{cm}^{-1}$ and $\chi_{22} = -0.9(4)\,\text{cm}^{-1}$ for the $\tilde{X}\,^2A_1$ state, as well as $\omega_2 = 386(4)\,\text{cm}^{-1}$ and $\chi_{22} = -0.9(1.3)\,\text{cm}^{-1}$ for the $\tilde{B}\,^2A_1$ state. Note that the relative energy ordering of the neutral states is clearly established by both experimental assignments and calculations, but neither can definitively establish the anion state.

B. Franck-Condon simulations

FC simulated spectra further confirm the assignments of the neutral states. Moreover, they can aid in identifying the anion state from which photodetachment occurs. The FC profiles for a given band should differ depending on the initial and final states, and the calculated bands from the two likely anion states can be compared to the experimental results to validate detachment from one of the two states to the three neutral states. The calculated bond lengths for the $^3B_1$ and $^3A_1$ states of VO_2^- in Table II are very similar, but the calculated bond angles differ by 2.2°. The calculated bond lengths and angles are slightly smaller for all three neutral states compared to the two anion states, but the change in bond angle for photodetachment to the $\tilde{A}\,^2B_1$ state is less than for photodetachment to the other two states, particularly when starting from the anion $^3B_1$ state. Simply on the basis of these geometry changes, we would expect all three bands to show some FC activity in the ν_1 and ν_2 modes, but with less ν_2 activity in the $\tilde{A}\,^2B_1$ band.

Stick spectra of calculated FC intensities are displayed in Fig. 4, showing simulated detachment spectra from the two triplet anion states to all three neutral states. All geometries, vibrational frequencies, and normal mode coordinates are those calculated at the BPW91/LANL2TZ level, with no fitting to match experimental results. The horizontal scale is the internal energy within a given electronic state, thus all vibrational origins are set to zero energy. The three different bands have characteristic FC profiles, regardless of the choice of anion state. The $\tilde{A}\,^2B_1$ simulated bands are the most distinct. They are dominated by the vibrational origin and show similar activity in the ν_1 mode. Considerably less activity is seen in the ν_2 mode, particularly in the simulation originating from the anion $^3B_1$ state (Fig. 4(b)). The $\tilde{X}\,^2A_1$ and $\tilde{B}\,^2A_1$ simulations each show significant activity in the ν_1 and ν_2 modes, as predicted. The ν_2 mode is considerably more active than the ν_1 modes the in the $\tilde{X}\,^2A_1$ band, while both modes contribute more equally to the $\tilde{B}\,^2A_1$ band. These trends hold regardless of anion state, but in general more ν_2 activity is seen from the $^3A_1$ state.

The FC profiles support the choice of the $^3B_1$ state as the anion ground state. In the $\tilde{X}$ band, the experimental 2_0^n progression peaks in intensity at $n = 2$. The most intense transition in the simulated $\tilde{X}\,^2A_1 \leftarrow {}^3B_1$ band is also the 2_0^2 transition, while that in the $\tilde{X}\,^2A_1 \leftarrow {}^3A_1$ simulation is the 2_0^3 transition. In the $\tilde{A}$ band, the experimental spectra show little activity in the ν_2 mode, with the intensity of the 2_0^1 transition (peak A2) at less than 10% that of the origin. This is consistent with the simulated $\tilde{A}\,^2B_1 \leftarrow {}^3B_1$ band, while the calculated $\tilde{A}\,^2B_1 \leftarrow {}^3A_1$ band has a relative intensity of 20% for the 2_0^1

transition. Finally, the most intense peak in the $\tilde{B}$ band is the vibrational origin, but the simulations predict the 2_0^1 and 2_0^2 transitions to be the most intense peaks for detachment from the $^3B_1$ and $^3A_1$ anion, respectively. Although the B3LYP calculations had no stable solution for the $\tilde{B}\,^2A_1$ state, analogous FC simulations for the first two neutral states have similar results, with more simulated FC activity in the ν_2 mode from the $^3A_1$ state relative to experiment. Overall, the ν_2 FC progressions for all three bands are better described by detachment from the $^3B_1$ state than the $^3A_1$ state, with the simulated spectra originating from the $^3A_1$ state consistently overpredicting the extent of FC activity in the ν_2 mode. The origin of this trend is clear from Table III, which shows a smaller change in bond angle upon detachment from the $^3B_1$ state to each of the three neutral states.

We therefore assign the $^3B_1$ state as the anion ground state and henceforth refer to it as the $\tilde{X}^3B_1$ state. Even though the two anion states are calculated to be very close in energy, there is no evidence for detachment from two anion states in our experiment, such as the observation of two bands in which the vibrational frequencies are identical. The combination of molecular beam expansion and ion trapping with cooling thus appears to have brought all the VO_2^- anions into their ground vibronic state.

C. Satellite bands

Regardless of the choice of starting anion state, one of the three photodetachment transitions seen here is forbidden in the one-electron approximation. Fig. 5 summarizes the situation. The left side shows the transitions from the $^3B_1$ anion state while the right side shows those from the $^3A_1$ state. If the anion is the $^3B_1$ state with the $\ldots(10a_1)^1(4b_1)^1$ electron configuration, accessing the $\tilde{B}\,^2A_1$ state would require a forbidden two-electron $(10a_1)^{-1}(4b_1)^{-1}(11a_1)^1$ detachment transition. Similarly, if the anion is in the $^3A_1$ state with the $\ldots(10a_1)^1(11a_1)^1$ configuration, photodetachment to the $\tilde{A}\,^2B_1$ state would require a $(10a_1)^{-1}(11a_1)^{-1}(4b_1)^1$ transition.

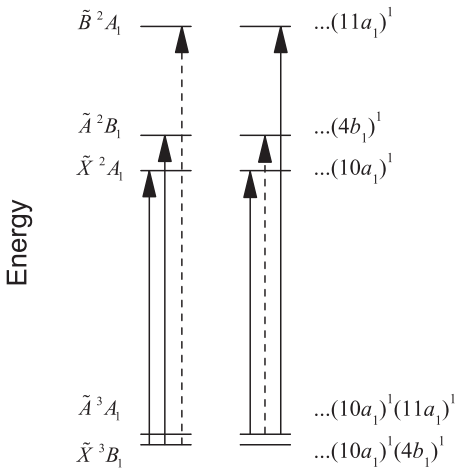

FIG. 5. Energy level diagram illustrating the transitions forbidden by the one-electron approximation. Solid arrows depict allowed one-electron detachment transitions, while dashed arrows are forbidden two-electron detachment transitions. The left side shows detachment from the $^3B_1$ anion state, and the right side shows detachment from the $^3A_1$ state. Energies are to scale with those from the BPW91/LANL2TZ calculations.

Although such satellite bands are nominally forbidden, they have been observed in photoionization experiments, primarily in core-level ionization but also in valence ionization.[74–76] Fewer such instances have been reported in anion photodetachment experiments, but two-electron transitions have been assigned in the anion PE spectra of Cu^-, ScO^-, and FeO^-.[77–79] These two-electron transitions have been attributed to configuration interaction in the product species between the allowed state and the forbidden state. Two-electron transitions can borrow intensity from allowed one-electron transitions of the same symmetry. Thus, if the $\tilde{B}\,^2A_1$ band is forbidden, it can borrow intensity from the nearby $\tilde{X}\,^2A_1$ state, while if the $\tilde{A}\,^2B_1$ band is forbidden, it can be seen only by borrowing intensity from a higher-lying allowed $^2B_1$ state with an electron configuration of $\ldots\ (3b_1)^1(10a_1)^1(11a_1)^1$, accessible from the $^3A_1$ state by a $(3b_1)^{-1}$ transition. Calculations at the BPW91/LANL2TZ level suggest that such a state lies 2.9 eV higher in energy than the $\tilde{A}\,^2B_1$ state. The considerably larger energy gap between the two $^2B_1$ states compared to the two $^2A_1$ states suggests that configuration interaction mixing is likely to be much less significant for the $^2B_1$ states.

Multireference calculations also support the existence of significant configuration interaction between the two $^2A_1$ states and less between the two $^2B_1$ states. Using the method outlined in Sec. IV, we calculated the state-averaged CASSCF configurations for the lowest-two $^2A_1$ and $^2B_1$ states. The lower $^2B_1$ state is dominated by a single configuration, the expected $\ldots(4b_1)^1$ configuration, with a coefficient of 0.88, or a weight of 77%. The second $^2B_1$ state has a coefficient of 0.70 of the expected $\ldots(3b_1)^1(10a_1)^1(11a_1)^1$ configuration corresponding to detachment from the lowest occupied b_1 orbital, but it has an insignificant contribution from the $\ldots(4b_1)^1$ configuration. In contrast, the lowest two $^2A_1$ states are heavily mixed. Both states are primarily composed of the $\ldots(10a_1)^1$ and $\ldots(11a_1)^1$ configurations, with the lower state having coefficients of -0.67 and 0.53 and the higher state with coefficients of 0.47 and 0.80, respectively. CASSCF calculations suggest considerable mixing between the two $^2A_1$ states and minimal mixing between the two $^2B_1$ states, and hence the $\tilde{B}\,^2A_1$ band is more likely to be the satellite band than the $\tilde{A}\,^2B_1$ band. These considerations further support our assignment of the $\tilde{X}\,^3B_1$ state as the anion ground state.

D. Comparison with prior reports

Previous experiments focusing on the VO_2 neutral ground state include EPR and IR spectroscopy of matrix-isolated VO_2. Detailed analysis of the EPR spectra of VO_2 in a neon matrix confirmed that the ground state is a $^2A_1$ state, in agreement with our theoretical and experimental assignments.[31] The IR spectra of VO_2 in an argon matrix yielded frequencies of 946.3 cm^{-1} and 935.9 cm^{-1} for the ν_1 and ν_3 vibrational fundamentals, respectively.[34] The ν_3 mode

is not active in photodetachment, but the value of the ν_1 fundamental is less than 1.5% off from our value of 960(3) cm^{-1}. Though this is a relatively large deviation, it is not uncommon for matrix-perturbed values compared to gas-phase values.[80] IR spectroscopy in a less-perturbing neon matrix, however, gave 958.0 cm^{-1} for the ν_1 vibrational fundamental, in almost exact agreement with our value.[39] Gas-phase vibrational frequencies of ground state VO_2 have also been obtained by a combination photoionization/photofragmentation study.[81] The 1_1^0 and 2_1^0 hot bands of an absorption feature were observed, yielding frequencies of 993.0 cm^{-1} and 296.0 cm^{-1} for the ν_1 and ν_2 fundamentals, respectively. These values are beyond the error bounds for our corresponding values of 960(3) cm^{-1} and 291(2) cm^{-1}, respectively.

The PE spectrum of the VO_2^- anion reported by Wu and Wang also showed detachment to the three neutral states as well as higher excited states, but at lower resolution and higher ion temperatures.[40] They observed three bands with onsets at ~15 000 cm^{-1}, 16 370(80) cm^{-1}, and 21 000(800) cm^{-1}. Within the reported error, these correspond to the reported onsets for the $\tilde{X}\,^2A_1$, $\tilde{A}\,^2B_1$, and $\tilde{B}\,^2A_1$ bands in this work. However, the intensity of the first band seemed to have some dependence on ion source conditions and was attributed to detachment from an electronically excited anion state. Consequently, the band that we assign to the $\tilde{A}\,^2B_1$ state was assigned as the transition to the neutral ground state in that work, and the EA was correspondingly assigned to the onset of that band, 2.03(1) eV. Similarly, the $\tilde{B}\,^2A_1$ band in this work was assigned as the $\tilde{A}\,^2B_1$ band, with a term energy of 0.6 eV.

The combination of high-resolution spectra with ion cooling compared with calculated energetics and FC simulations allows us to say with confidence that peak X1 represents the vibrational origin of the ground electronic state and thus that the EA is 1.8357(5) eV. The dependence of the first band on source conditions in the earlier PE experiment is possibly due to overlap with a lower-lying band with an onset at 13 900(200) cm^{-1}. This band was also attributed to an excited anion state, and may be from detachment from the $\tilde{A}\,^3A_1$ anion. Given that our calculated FC profile for that transition is ~3000 cm^{-1} wide, that band may overlap with that of the ground state band and could have caused the apparent dependence on ion source conditions.

In the earlier PE spectrum, vibrational frequencies were only obtained for the $\tilde{A}\,^2B_1$ band, which exhibited a short progression of 970(40) cm^{-1}. This spacing was originally assigned as the ν_1 frequency of the $\tilde{X}\,^2A_1$ state, but is consistent with the ν_1 frequency of the $\tilde{A}\,^2B_1$ state in our work.

VI. CONCLUSION

High-resolution photoelectron spectra, obtained by a combination of cryogenic ion cooling and SEVI spectroscopy, are obtained of the vanadium dioxide anion. The improved resolution and low ion temperature allows for an accurate determination of the VO_2 electron affinity and the term energies of its lowest two excited states. The ν_1 and ν_2 vibrational frequencies are also obtained for all three neutral VO_2 states. The calculated energetics, FC profiles, and observed satellite peaks all suggest that the anion ground state is the $\tilde{X}\,^3B_1$ state and not the energetically close $\tilde{A}\,^3A_1$ state.

Even relatively simple d^1 and d^2 transition metal systems, such as neutral and anion VO_2, can have several low-lying electronic states, and disentangling them from each other requires careful use of a high-resolution technique like SEVI. Understanding the vibronic structure of model systems of catalytic active sites is not a straightforward task. Theoretical methods are still being developed to bring the accuracy of transition metal computational chemistry to the level that has been accomplished for main group chemistry. Relatively few experimental spectroscopic techniques are available for studying the vibronic structure of size-selected clusters, and new approaches like cryo-cooled SEVI show promise for elucidating the vibronic structure of more complex systems than studied in detail before.

ACKNOWLEDGMENTS

This work is funded by the Air Force Office of Scientific Research under Grant No. FA9550-12-1-0160 and the Defense University Research Instrumentation Program under Grant No. FA9550-11-1-0330. M.L.W. thanks the National Science Foundation for a graduate research fellowship.

[1] B. M. Weckhuysen and D. E. Keller, Catal. Today **78**, 25 (2003).
[2] G. C. Bond and S. F. Tahir, Appl. Catal. **71**, 1 (1991).
[3] A. Khodakov, B. Olthof, A. T. Bell, and E. Iglesia, J. Catal. **181**, 205 (1999).
[4] L. J. Burcham, L. E. Briand, and I. E. Wachs, Langmuir **17**, 6164 (2001).
[5] A. Cavalleri, M. Rini, H. H. W. Chong, S. Fourmaux, T. E. Glover, P. A. Heimann, J. C. Kieffer, and R. W. Schoenlein, Phys. Rev. Lett. **95**, 067405 (2005).
[6] Z. Yang, C. Ko, and S. Ramanathan, Annu. Rev. Mater. Res. **41**, 337 (2011).
[7] J. H. Park, J. M. Coy, T. S. Kasirga, C. Huang, Z. Fei, S. Hunter, and D. H. Cobden, Nature (London) **500**, 431 (2013).
[8] D. Göbke, Y. Romanyshyn, S. Guimond, J. M. Sturm, H. Kuhlenbeck, J. Döbler, U. Reinhardt, M. V. Ganduglia-Pirovano, J. Sauer, and H.-J. Freund, Angew. Chem., Int. Ed. **48**, 3695 (2009).
[9] A. Goodrow, A. T. Bell, and M. Head-Gordon, J. Phys. Chem. C **113**, 19361 (2009).
[10] H. Y. Kim, H. M. Lee, and H. Metiu, J. Phys. Chem. C **114**, 13736 (2010).
[11] H. Häkkinen, S. Abbet, A. Sanchez, U. Heiz, and U. Landman, Angew. Chem., Int. Ed. **42**, 1297 (2003).
[12] U. Heiz and E. L. Bullock, J. Mater. Chem. **14**, 564 (2004).
[13] K. A. Zemski, D. R. Justes, and A. W. Castleman, J. Phys. Chem. B **106**, 6136 (2002).
[14] K. R. Asmis and J. Sauer, Mass Spectrom. Rev. **26**, 542 (2007).
[15] S. Feyel, D. Schröder, X. Rozanska, J. Sauer, and H. Schwarz, Angew. Chem., Int. Ed. **45**, 4677 (2006).
[16] N. Magg, B. Immaraporn, J. B. Giorgi, T. Schroeder, M. Bäumer, J. Döbler, Z. Wu, E. Kondratenko, M. Cherian, M. Baerns, P. C. Stair, J. Sauer, and H.-J. Freund, J. Catal. **226**, 88 (2004).
[17] M. Engeser, M. Schlangen, D. Schröder, H. Schwarz, T. Yumura, and K. Yoshizawa, Organometallics **22**, 3933 (2003).
[18] M. Engeser, D. Schröder, and H. Schwarz, Chem. Eur. J. **11**, 5975 (2005).
[19] J. N. Harvey, M. Diefenbach, D. Schröder, and H. Schwarz, Int. J. Mass Spectrom. **182–183**, 85 (1999).
[20] F. Dong, S. Heinbuch, Y. Xie, J. J. Rocca, and E. R. Bernstein, J. Phys. Chem. A **113**, 3029 (2009).
[21] S. Yin and E. R. Bernstein, Int. J. Mass Spectrom. **321–322**, 49 (2012).
[22] Z.-C. Wang, S. Yin, and E. R. Bernstein, Phys. Chem. Chem. Phys. **15**, 10429 (2013).
[23] M. Zhou, C. Wang, J. Zhuang, Y. Zhao, and X. Zheng, J. Phys. Chem. A **115**, 39 (2011).
[24] X. Zhou, M. Chen, and M. Zhou, J. Phys. Chem. A **117**, 5463 (2013).
[25] C. J. Cramer and D. G. Truhlar, Phys. Chem. Chem. Phys. **11**, 10757 (2009).

[26]Y. Kurashige and T. Yanai, J. Chem. Phys. **130**, 234114 (2009).
[27]G. Santambrogio, M. Brümmer, L. Wöste, J. Döbler, M. Sierka, J. Sauer, G. Meijer, and K. R. Asmis, Phys. Chem. Chem. Phys. **10**, 3992 (2008).
[28]D. Schröder, S. Shaik, and H. Schwarz, Acc. Chem. Res. **33**, 139 (2000).
[29]A. J. Merer, Annu. Rev. Phys. Chem. **40**, 407 (1989).
[30]W. S. Hopkins, S. M. Hamilton, and S. R. Mackenzie, J. Chem. Phys. **130**, 144308 (2009).
[31]L. B. Knight, R. Babb, M. Ray, T. J. Banisaukas, L. Russon, R. S. Dailey, and E. R. Davidson, J. Chem. Phys. **105**, 10237 (1996).
[32]G. L. Gutsev, B. K. Rao, and P. Jena, J. Phys. Chem. A **104**, 11961 (2000).
[33]E. Jakubikova, A. K. Rappé, and E. R. Bernstein, J. Phys. Chem. A **111**, 12938 (2007).
[34]G. V. Chertihin, W. D. Bare, and L. Andrews, J. Phys. Chem. A **101**, 5090 (1997).
[35]M. Calatayud, B. Silvi, J. Andrés, and A. Beltrán, Chem. Phys. Lett. **333**, 493 (2001).
[36]E. L. Uzunova, H. Mikosch, and G. S. Nikolov, J. Chem. Phys. **128**, 094307 (2008).
[37]S. F. Vyboishchikov and J. Sauer, J. Phys. Chem. A **104**, 10913 (2000).
[38]A. Bande and A. Lüchow, Phys. Chem. Chem. Phys. **10**, 3371 (2008).
[39]Y. Gong, M. Zhou, and L. Andrews, Chem. Rev. **109**, 6765 (2009).
[40]H. Wu and L.-S. Wang, J. Chem. Phys. **108**, 5310 (1998).
[41]M. Brümmer, C. Kaposta, G. Santambrogio, and K. R. Asmis, J. Chem. Phys. **119**, 12700 (2003).
[42]D. M. Neumark, J. Phys. Chem. A **112**, 13287 (2008).
[43]C. Hock, J. B. Kim, M. L. Weichman, T. I. Yacovitch, and D. M. Neumark, J. Chem. Phys. **137**, 244201 (2012).
[44]H. J. Zhai and L. S. Wang, Chem. Phys. Lett. **500**, 185 (2010).
[45]J. E. Mann, N. J. Mayhall, and C. C. Jarrold, Chem. Phys. Lett. **525–526**, 1 (2012).
[46]A. Osterwalder, M. J. Nee, J. Zhou, and D. M. Neumark, J. Chem. Phys. **121**, 6317 (2004).
[47]A. T. J. B. Eppink and D. H. Parker, Rev. Sci. Instrum. **68**, 3477 (1997).
[48]M. B. Doyle, C. Abeyasera, and A. G. Suits, NuACQ, 2012, see http://chem.wayne.edu/suitsgroup/NuACQ.html.
[49]E. W. Hansen and P.-L. Law, J. Opt. Soc. Am. A **2**, 510 (1985).
[50]C. Blondel, W. Chaibi, C. Delsart, C. Drag, F. Goldfarb, and S. Kröger, Eur. Phys. J. D **33**, 335 (2005).
[51]C. Blondel, W. Chaibi, C. Delsart, and C. Drag, J. Phys. B: At., Mol. Opt. Phys. **39**, 1409 (2006).
[52]E. P. Wigner, Phys. Rev. **73**, 1002 (1948).
[53]J. B. Kim, M. L. Weichman, and D. M. Neumark, Phys. Chem. Chem. Phys. **15**, 20973 (2013).
[54]J. B. Kim, M. L. Weichman, T. I. Yacovitch, C. Shih, and D. M. Neumark, J. Chem. Phys. **139**, 104301 (2013).
[55]M. L. Weichman, J. B. Kim, and D. M. Neumark, J. Chem. Phys. **139**, 144314 (2013).
[56]J. Cooper and R. N. Zare, J. Chem. Phys. **48**, 942 (1968).
[57]K. L. Reid, Annu. Rev. Phys. Chem. **54**, 397 (2003).
[58]C. Bartels, C. Hock, J. Huwer, R. Kuhnen, J. Schwöbel, and B. von Issendorff, Science **323**, 1323 (2009).
[59]A. J. Merer, G. Huang, A. S. C. Cheung, and A. W. Taylor, J. Mol. Spectrosc. **125**, 465 (1987).
[60]R. S. Mulliken, J. Chem. Phys. **23**, 1997 (1955).
[61]A. D. Becke, Phys. Rev. A **38**, 3098 (1988).
[62]J. P. Perdew, J. A. Chevary, S. H. Vosko, K. A. Jackson, M. R. Pederson, D. J. Singh, and C. Fiolhais, Phys. Rev. B **46**, 6671 (1992).
[63]A. D. Becke, J. Chem. Phys. **98**, 5648 (1993).
[64]K. R. Asmis, G. Meijer, M. Brümmer, C. Kaposta, G. Santambrogio, L. Wöste, and J. Sauer, J. Chem. Phys. **120**, 6461 (2004).
[65]S. F. Vyboishchikov and J. Sauer, J. Phys. Chem. A **105**, 8588 (2001).
[66]P. J. Hay and W. R. Wadt, J. Chem. Phys. **82**, 299 (1985).
[67]L. E. Roy, P. J. Hay, and R. L. Martin, J. Chem. Theory Comput. **4**, 1029 (2008).
[68]A. T. B. Gilbert, N. A. Besley, and P. M. W. Gill, J. Phys. Chem. A **112**, 13164 (2008).
[69]Y. Shao, L. F. Molnar, Y. Jung, J. Kussmann, C. Ochsenfeld, S. T. Brown, A. T. B. Gilbert, L. V. Slipchenko, S. V. Levchenko, D. P. O'Neill, R. A. DiStasio Jr, R. C. Lochan, T. Wang, G. J. O. Beran, N. A. Besley, J. M. Herbert, C. Yeh Lin, T. Van Voorhis, S. Hung Chien, A. Sodt, R. P. Steele, V. A. Rassolov, P. E. Maslen, P. P. Korambath, R. D. Adamson, B. Austin, J. Baker, E. F. C. Byrd, H. Dachsel, R. J. Doerksen, A. Dreuw, B. D. Dunietz, A. D. Dutoi, T. R. Furlani, S. R. Gwaltney, A. Heyden, S. Hirata, C.-P. Hsu, G. Kedziora, R. Z. Khalliulin, P. Klunzinger, A. M. Lee, M. S. Lee, W. Liang, I. Lotan, N. Nair, B. Peters, E. I. Proynov, P. A. Pieniazek, Y. Min Rhee, J. Ritchie, E. Rosta, C. David Sherrill, A. C. Simmonett, J. E. Subotnik, H. Lee Woodcock III, W. Zhang, A. T. Bell, A. K. Chakraborty, D. M. Chipman, F. J. Keil, A. Warshel, W. J. Hehre, H. F. Schaefer III, J. Kong, A. I. Krylov, P. M. W. Gill, and M. Head-Gordon, Phys. Chem. Chem. Phys. **8**, 3172 (2006).
[70]H. J. Werner, P. J. Knowles, G. Knizia, F. R. Manby, M. Schütz *et al.*, MOLPRO, version 2010.1, a package of *ab initio* programs, 2010, see http://www.molpro.net.
[71]V. A. Mozhayskiy and A. I. Krylov, ezSpectrum, 2009, see http://iopenshell.usc.edu/downloads.
[72]F. Duschinsky, Acta Physicochim. URSS **7**, 551 (1937).
[73]L.-S. Wang, in *Photoionization and Photodetachment*, edited by C. Y. Ng (World Scientific, Singapore, 2000), Vol. 10.
[74]A. W. Potts and T. A. Williams, J. Electron Spectrosc. Relat. Phenom. **3**, 3 (1974).
[75]L. S. Cederbaum, W. Domcke, J. Schirmer, and W. V. Niessen, in *Advances in Chemical Physics*, edited by I. Prigogine and S. A. Rice (John Wiley & Sons, Inc., 1986), p. 115.
[76]S. Süzer, S. T. Lee, and D. A. Shirley, Phys. Rev. A **13**, 1842 (1976).
[77]H. Wu and L.-S. Wang, J. Phys. Chem. A **102**, 9129 (1998).
[78]G. Drechsler, U. Boesl, C. Bäßmann, and E. W. Schlag, J. Chem. Phys. **107**, 2284 (1997).
[79]H. Wu, S. R. Desai, and L.-S. Wang, J. Phys. Chem. A **101**, 2103 (1997).
[80]M. E. Jacox, J. Phys. Chem. Ref. Data **13**, 945 (1984).
[81]Y. Matsuda and E. R. Bernstein, J. Phys. Chem. A **109**, 3803 (2005).